Advances in Science and Technology Research Journal

Advances in Science and Technology Research Journal, 2026, 20(10), 132–146
https://doi.org/10.12913/22998624/224520
ISSN 2299-8624, License CC-BY 4.0

Received: 2026.05.18
Accepted: 2026.07.13
Published: 2026.09.01

Computational fluid dynamics-based comparative assessment of inlet location in a modular water-curtain head for robotic abrasive blasting

Paweł Pac[1], Agnieszka Sękala[2*], Dariusz Prostański[3]

[1] PONAR Wadowice S.A., Św. Jana Pawła II 10, 43-170 Łaziska Górne, Poland
[2] Silesian University of Technology, Faculty of Mechanical Engineering, Konarskiego 18A 44-100 Gliwice, Poland
[3] KOMAG Institute of Mining Technology, Pszczyńska 37, 44-101 Gliwice, Poland
* Corresponding author's e-mail: agnieszka.sekala@polsl.pl

ABSTRACT

Steel surface preparation processes in the shipbuilding industry based on abrasive blasting generate high dust concentrations, including the hazardous respirable fraction. The present study focuses on the computational fluid dynamics (CFD) assisted design assessment of a modular water-curtain head integrated with the cleaning module of a mobile magnetic robot used in abrasive blasting. The proposed solution is intended to reduce pollutant emissions at source while maintaining the low mass, compact geometry and serviceability required for robotic operation on ferromagnetic surfaces. Comparative numerical analyses were carried out using ANSYS CFX for two design variants of the supply manifold, differing in the position of the inlet relative to the nozzle channels. The study focused on flow stability, pressure distribution and the uniformity of mass flow rate across six full-cone spray nozzles. The results showed that the inlet location affected the hydraulic balance of the manifold and the uniformity of nozzle supply. The configuration with the inlet located between the nozzle channels provided a more uniform distribution of the working medium, whereas the configuration with the inlet adjacent to one nozzle channel generated stronger local asymmetry in the inlet region. The results indicate that comparative CFD analysis can effectively support the design of compact spraying heads for robotic abrasive blasting systems.

Keywords: abrasive blasting, mobile magnetic robot, water-curtain head, computational fluid dynamics, flow distribution, dust suppression, respirable dust.

INTRODUCTION

The refurbishment of large-scale steel structures, such as ship hulls and storage tanks, relies primarily on abrasive blasting methods. In ship repair yards, abrasive blasting remains widely used because it enables efficient surface preparation at relatively low operating costs. However, the process generates high concentrations of airborne dust, including respirable fractions. Although copper slag is commonly regarded as safer than quartz sand because of its low free silica content, its disintegration during impact with the treated surface may generate fine dust containing heavy metals and particles smaller than 5 µm. These particles can penetrate deep into the respiratory tract of operators [1].

Surface preparation is particularly important in the maritime sector, where protective coatings on ship hulls protect against corrosion, fire-related hazards and biofouling but degrade under harsh environmental conditions. Periodic dry-docking and coating renewal require the removal of old paint layers, rust and surface contaminants, most commonly by abrasive blasting [1]. This process generates substantial quantities of spent abrasive and paint residues. T may lmit the usabilityhe quantity of abrasive blasting media waste may range from 20 to 200 kg/m^2 of cleaned surface, with typical values of 40–50 kg/m^2. This waste may contain toxic components originating from both the abrasive medium and the removed antifouling coatings [1].

Environmental and occupational safety requirements have increased interest in techniques for reducing dust emissions at source. Wet abrasive blasting and slurry blasting can reduce airborne dust, but they introduce additional wastewater and sludge streams that must be collected and treated. Ultra-high pressure water jetting can reduce the mass of solid waste, but it may generate toxic paint sludge containing elevated concentrations of metals such as copper and zinc [1]. Therefore, in shipyard applications, a dust-suppression system should reduce airborne emissions while limiting water consumption, waste generation, added mass and maintenance requirements.

The use of mobile and semi-automated systems for abrasive blasting introduces additional design constraints. Mobile magnetic robots intended to operate on ferromagnetic surfaces must maintain stable adhesion and mobility on vertical, inclined or inverted structures. Consequently, any additional equipment mounted on the robot, including spraying or shielding systems, must be lightweight and compact while ensuring sufficient operational reliability. Excessive weight, complex auxiliary systems or sensitivity to contamination of the water supply may limit the usability of the robotic platform under shipyard conditions. For this reason, the design of water-curtain heads for mobile abrasive-blasting robots requires a balance between hydraulic performance, serviceability and structural simplicity.

Several dust-suppression mechanisms have been reported in the literature, including the use of nanofluids to improve wetting and the use of magnetised or charged droplets [2, 3]. The use of surfactants to improve wetting and agglomeration, as well as composite dust suppressants, has also been investigated [4, 5]. Recent research has also focused on systems for mitigating submicron dust, foam-air curtain arrangements, and negative-pressure-assisted supersonic atomisation [6–8]. These approaches can improve the capture of fine particles under selected conditions. However, their implementation in mobile robotic systems may be limited by the need for additional dosing, charging or flow-control devices, as well as by increased mass and maintenance complexity. In abrasive blasting applications, the working environment is also characterised by dust exposure and variable water quality, which may affect the durability of fine atomising components. Macroscopic spray visualisation studies make it possible to assess spray penetration and spray angle [9]. Studies on ultrasonic dry-fog nozzles have examined the relationship between operating conditions, atomisation characteristics, and dust-suppression efficiency [10]. Device-oriented studies have also investigated magnetised water spray devices and plasma-activated supersonic water fog [11, 12].

These spray characteristics are relevant to maintaining a continuous protective water barrier near the abrasive discharge zone. At the same time, spraying systems intended for abrasive-blasting robots should use nozzle designs that are resistant to clogging, easy to replace and suitable for operation under standard industrial water-supply conditions. This requirement favours mechanically robust and serviceable designs over highly sensitive atomising systems.

Computational fluid dynamics is widely used to support the analysis and optimisation of spraying and dust suppression systems. Numerical models enable the assessment of flow fields and dust-suppression performance prior to prototype testing [13, 14]. Further studies have investigated wind-assisted electrospraying, CFD-based dust–droplet coupling for the control of dust generated by tunnel blasting and wind-fog coupling in tunnel drilling and blasting operations [15–17]. The influence of nozzle structure on atomisation characteristics, as well as the wind-responsive adjustment of dust-suppression parameters, has also been examined [18, 19]. CFD methods have also been applied to the design of spray dust control devices [20]. Studies of multi-nozzle headers in other fluid systems have shown that header geometry affects outlet flow uniformity [21]. However, compact water-curtain heads dedicated to mobile magnetic robots used in abrasive blasting remain insufficiently described, particularly with respect to hydraulic balance and nozzle-supply repeatability under strict mass and serviceability constraints.

The present work continues the authors' research on numerical methods supporting the development of mobile magnetic robotic systems. Previous studies by the authors concerned finite element post-processing and topology-based mass reduction [22, 23]. Subsequent work focused on the validation of robot-frame models using virtual strain gauges [24, 25]. In the present study, the focus shifts from the load-bearing structure of the robot to the hydraulic behaviour of a modular water-curtain head integrated with the cleaning module. The analysed head uses six full-cone spray nozzles supplied by a compact manifold intended to generate a water barrier near the abrasive discharge zone.

The aim of this study is to assess how the inlet position in the supply manifold affects flow stability, pressure distribution and the uniformity of mass flow rate through individual nozzles. Two design variants were analysed using ANSYS CFX under identical boundary conditions and mesh settings. The results are intended to support the selection of a manifold configuration suitable for a mobile magnetic robot used in abrasive blasting, with particular attention to hydraulic balance, compactness and operational reliability.

MATERIALS AND METHODS

The robotic system designed to support specialised operations (Figure 1) is an advanced mobile platform developed for operation under demanding industrial conditions, including operation on surfaces covered with thick corrosion layers and environments with high concentrations of respirable dust. One of its main functional features is the ability to move on ferromagnetic surfaces in any spatial orientation.

A key component of the platform is a hybrid locomotion system integrated with a magnetic adhesion system, which enables stable motion on vertical and inverted ferromagnetic surfaces, such as ship hulls and large-scale storage tanks. The platform combines an abrasive blasting module (Figure 2a) with a water-curtain system intended to reduce pollutant emissions at source. This solution addresses the need to limit dust dispersion during surface preparation while maintaining compatibility with the operational constraints of a mobile magnetic robot.

The modular water-curtain head (Figure 2b) was designed to combine low structural mass and compact geometry with the stable generation of a protective water barrier. The system is based on a supply manifold feeding six full-cone nozzles fitted with a G1/8″ thread. This arrangement enables the spraying parameters to be selected according to the abrasive blasting conditions and the required dust-suppression intensity. The internal channel geometry was assessed using CFD simulations performed using ANSYS CFX. The analysis focused on the occurrence of stagnation zones and the uniformity of the mass-flow-rate distribution across the outlets, as these factors are important for maintaining the continuity and stability of the generated water curtain under operating conditions.

The design procedure for the water-curtain head included the development of a three-dimensional model, preparation of the fluid domain, CFD analysis of the internal flow, and assessment of the pressure drop and flow-rate distribution across the nozzles. The analysed configurations differed in the position of the inlet connector relative to the nozzle channels. In variant A, the working medium was supplied adjacent to the first nozzle channel, whereas in variant B, the inlet was located between the nozzle channels. The comparison was intended to assess whether the proposed compact manifold geometry could provide stable and repeatable outlet-flow conditions for all six nozzles. The number of nozzles was selected to balance the limits on total water

(a) (b)

Figure 1. Robotic system for supporting specialised operations on ferromagnetic surfaces (Polish Patent No. P.436523): (a) rendering of version 5.0; (b) photograph of version 4.0 during operation

(a) (b)

Figure 2. Cleaning module of the magnetic robot with the spray head for water-curtain generation indicated (Polish Patent Application No. P.451835): (a) view of the cleaning module; (b) water-curtain head

consumption, as defined by shipyard operating requirements, with the need to ensure sufficient overlap between the spray cones to form a continuous and stable water curtain.

At the prototype stage, the head was designed to use commercially available G1/8″ full-cone nozzles mounted in a modular body. This approach enables the nozzle parameters to be selected according to the required water-curtain characteristics and the permissible water consumption. The adopted modular design also enables the numerical results to be verified experimentally by flow-rate measurements and spray-pattern observations.

Wet abrasive blasting can reduce airborne dust, but its use in shipyard robotic applications is limited by additional water supply requirements, wastewater and sludge generation, increased system mass and higher maintenance demands. Therefore, the proposed solution was developed as a compact water-curtain head intended to suppress dust near the working zone without modifying the abrasive blasting process itself. Commercial wet blasting heads offer an alternative solution in which water is introduced near the blasting nozzle to reduce dust dispersion. However, such systems increase the complexity of the supply system, often require an additional pump and a high-pressure water supply, and may reduce serviceability. They can also increase water consumption and generate additional liquid waste. Under shipyard conditions, component wear, contaminant deposition and clogging of water nozzles may further limit operational durability. Therefore, for a mobile magnetic robot, the dust-suppression system should combine emission reduction with compact geometry, low mass, simple assembly and ease of maintenance.

Figure 3a shows the cleaning module of version 4.0 of the magnetic robot, equipped with four oscillating nozzles and a dedicated water-injection head mounted between the abrasive supply hose and the working unit. The head introduces water near the abrasive discharge zone in order to reduce dust emissions without modifying the basic abrasive blasting process.

The single nozzle-head assembly, which represents the basic working unit of the earlier system, is shown in cross-section in Figure 3b. In this configuration, each abrasive blasting nozzle was equipped with an individual water-injection system, enabling local dust suppression in the abrasive-jet impact zone. Operational experience with this solution showed, however, that its durability was limited, as the water nozzles required replacement after a relatively short service period. This indicated the need for a more robust and serviceable design adapted to the requirements of a mobile magnetic robot. In the proposed approach, the water-curtain head is not intended to modify the abrasive blasting process itself, but to provide an additional protective barrier that limits dust dispersion near the working zone.

The water-curtain head developed for robotic abrasive blasting is shown in Figure 4. The design was adapted to the constraints of a mobile magnetic robot, with particular attention paid to reduced mass, compact dimensions, ease of handling and operational durability. The head uses replaceable spray nozzles with a standard G1/8″ thread, allowing the nozzle diameter to be selected according to the required water-curtain

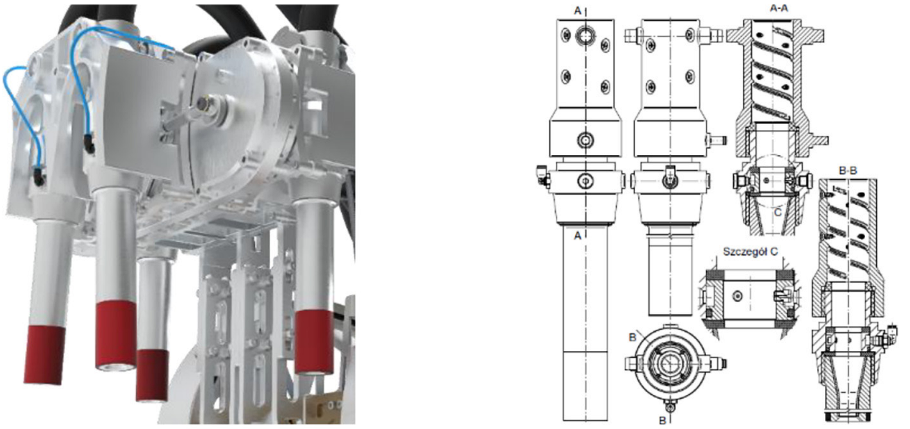

(a) (b)

Figure 3. Cleaning module of the magnetic robot: (a) four abrasive blasting nozzles with spray heads; (b) single abrasive blasting nozzle combined with a spray head

characteristics and permissible water consumption. The modular structure provides access to the internal channels after removal of the circlip and enables replacement of the sealing rings. The solution is based mainly on commercially available components, while the custom-manufactured components are limited to two body elements. The geometry includes six seats for full-cone nozzles and was developed to provide a stable water curtain while maintaining low system mass.

The water-curtain head was designed to use commercially available FullJet® B1/8HH-2 full-cone nozzles with a standard G1/8″ thread [26]. The internal swirl element supports the formation of a full-cone spray with uniform droplet distribution. According to the manufacturer's data, the nozzle operates within a pressure range of 0.4–10 bar and provides a flow rate of 0.59–2.6 L/min. This allows the nozzle parameters to be selected according to the required water-curtain characteristics and permissible water consumption.

The selected nozzle arrangement was intended to generate a protective water barrier near the abrasive discharge zone without modifying the abrasive blasting process itself. The modular head design allows replacement of the nozzles and sealing elements, facilitates maintenance and supports adaptation of the water consumption to the operating conditions of the robotic system.

To assess the hydraulic performance of the developed head, the fluid domain was prepared in Solid Edge 2020 Classic and analysed in ANSYS CFX. Two inlet-location variants were compared with respect to pressure losses, flow distribution and the uniformity of nozzle supply.

Both variants (Figure 5) were discretised using comparable unstructured tetrahedral meshes with local refinement in regions of curvature, constrictions and geometric transitions, where

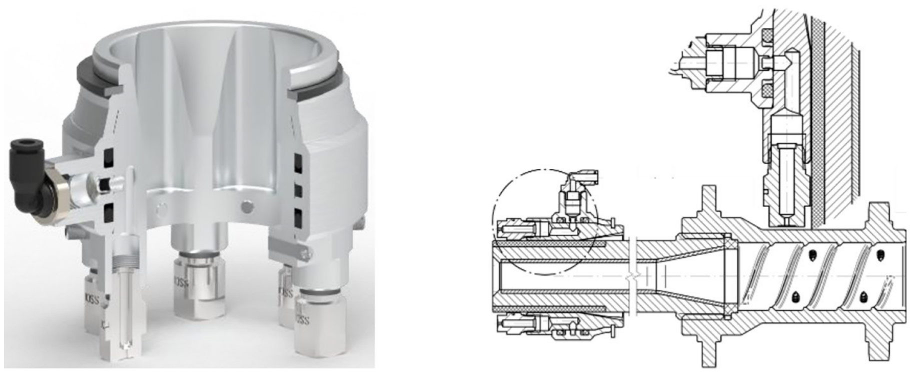

(a) (b)

Figure 4. Head developed for the magnetic robot: (a) 3D visualisation; (b) cross-section

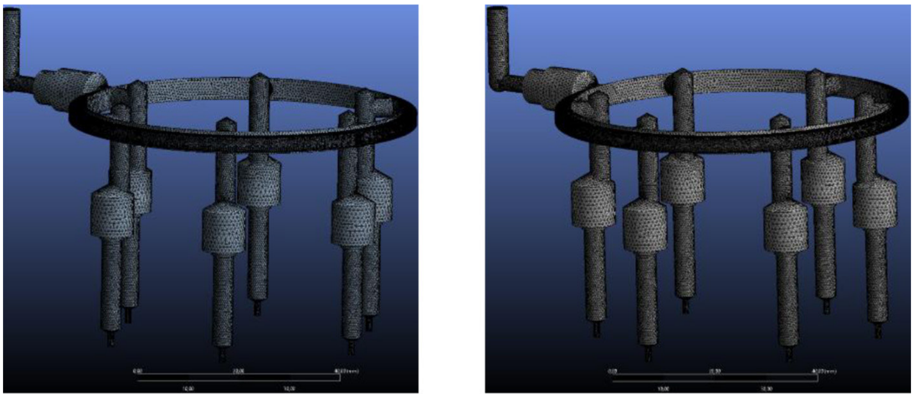

(a) (b)

Figure 5. Mesh in isometric view: (a) inlet channel adjacent to one of the nozzle channels; (b) inlet channel located between the nozzle channels

higher flow-field gradients were expected. The mesh density in the inlet region and in the branches leading to the nozzles was kept similar for both configurations. Therefore, differences observed in the numerical results can be related primarily to the change in inlet location rather than to differences in discretisation.

The water-inlet region is important because the flow begins to divide between the branches leading to the individual nozzles before entering the main manifold, as shown in Figure 6. In variant A, the inlet is positioned adjacent to one of the nozzle channels, which results in a more directional flow path near the first bifurcation. In variant B, the inlet is located between the nozzle channels, giving a more symmetrical arrangement with respect to the manifold axis. In both cases, mesh continuity was maintained in the regions of bends and geometric transitions, where increased pressure and velocity gradients were expected.

The nozzle inlet channel is another region relevant to the reliability of the numerical model, as it affects the uniformity of medium supply to the nozzle seat and the local hydraulic losses before the outlet (Figure 7). In both variants, the mesh was refined near the channel walls and in regions of geometric transition, where increased velocity gradients and local flow acceleration were expected. The discretisation quality in this region remained comparable for both configurations, indicating that the change in inlet location did not adversely affect the mesh representation of the nozzle inlet channels.

The mesh parameters and quality indicators for both configurations are summarised in Table 1. Both variants were based on the same fluid-domain volume and a comparable level of discretisation, with approximately 554,000 nodes and 1.35 million elements. Identical global mesh settings were applied, including curvature-based sizing, local refinement and

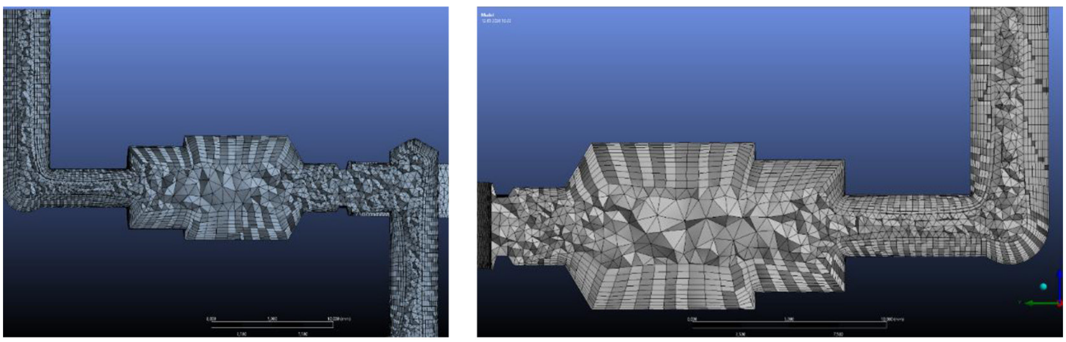

(a) (b)

Figure 6. Mesh cross-section through the water inlet: (a) inlet channel adjacent to one of the nozzle channels; (b) inlet channel located between the nozzle channels

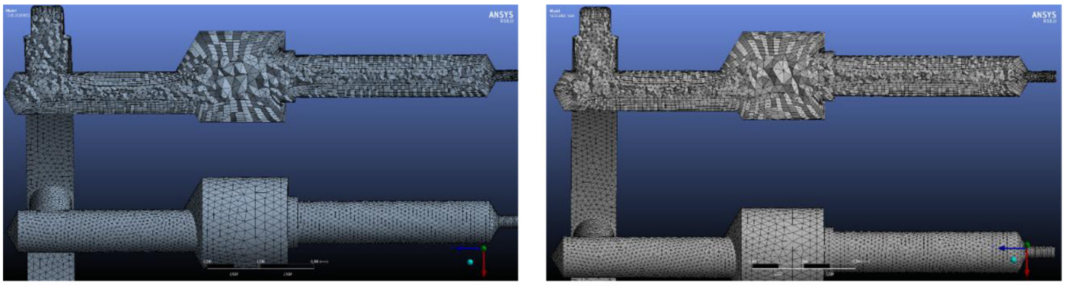

(a) (b)

Figure 7. Mesh cross-section through the nozzle inlet channel: (a) inlet channel adjacent to one of the nozzle channels; (b) inlet channel located between the nozzle channels

automatic boundary-layer generation. The average skewness values were similar for both configurations, indicating comparable mesh quality on the global scale. Local maximum skewness values were associated with individual cells in regions of pronounced geometric variation; however, these regions did not dominate the computational domain. The mesh quality was therefore considered suitable for the comparative assessment of the two inlet configurations. The adopted mesh and model parameters were kept consistent for both configurations to ensure that the comparison reflected the influence of inlet location.

Table 1. Summary of configuration parameters and mesh quality

Parameter	(a) Inlet channel adjacent to the first nozzle channel	(b) Inlet channel between nozzle channels I and II
Geometry		
Volume	8921.4 mm^3	8921.4 mm^3
Mesh statistics		
Number of nodes	553,932	554,314
Number of elements	1,353,456	1,353,751
Global settings		
Physics preference / solver preference	CFD / CFX	CFD / CFX
Relevance center	Fine	Fine
Element midside nodes	Dropped	Dropped
Sizing		
Size function	Curvature	Curvature
Min size	0.20 mm	0.20 mm
Max face size	1.20 mm	1.20 mm
Max tet size	1.50 mm	1.50 mm
Growth rate	1.150	1.150
Quality		
Mesh metric	Skewness	Skewness
Min skewness	1.071e-003	4.7964e-004
Max skewness	0.97112	0.97646
Average skewness	0.33978	0.33807
Standard deviation	0.17241	0.17236
Inflation		
Use automatic inflation	Program controlled	Program controlled
Inflation option	Smooth transition	Smooth transition
Maximum layers	10	10
Growth rate (inflation)	1.2	1.2

The boundary conditions applied in the CFX computational domain are shown in Figure 8 for the two analysed inlet configurations. In configuration A, the inlet was positioned adjacent to the channel leading to the first nozzle, whereas in configuration B, it was located between the channels leading to the left and right nozzle branches. This difference affects the initial division of the flow within the manifold. Configuration A provides a shorter supply path to the nearest branch and may therefore promote local flow asymmetry. Configuration B represents a more centrally supplied arrangement, which is expected to support a more balanced distribution of the working medium. The comparison of these two configurations was used to assess the influence of inlet location on the uniformity of nozzle supply.

The simulation setup adopted for both model variants is summarised in Table 2. A steady-state, isothermal analysis was performed for water at 18 °C using the k-ε turbulence model with scalable wall functions. The High Resolution advection scheme and an RMS convergence criterion of 1.0 × 10^{-4} were applied. Identical boundary conditions and solver settings were used for both configurations, including an inlet total pressure of 6 bar and an outlet average static pressure of 0 bar. This ensured that the comparison reflected the influence of inlet location rather than differences in numerical setup.

The same numerical setup was applied to both configurations so that the influence of factors unrelated to geometry was limited. As a result, differences in the obtained flow parameters can be attributed primarily to the change in inlet position.

The volumetric flow rate at each nozzle outlet was calculated from the corresponding mass flow rate according to Equation 1. The outlet flow rates were then used to compare the uniformity of nozzle supply, while the total flow rate was determined as the sum of the individual outlet values. This enabled both local differences between nozzles and the overall flow balance of the head to be assessed. The volumetric flow rate at each outlet is calculated according to the following equation [27]:

$$Q_i = \frac{|\dot{m}_i|}{\rho_w} \cdot 60{,}000 \tag{1}$$

where: Q_i – volumetric flow rate at outlet i, [L/min], $\dot{m}_i$ – mass flow rate at outlet i, [kg/s], ρ_w – water density [kg/m^3]; ρ_w = 998.2 kg/m^3.

The monitoring points were defined to evaluate both the flow rate at individual nozzle outlets and the total flow rate of the head. This made it possible to assess local non-uniformity in nozzle supply as well as the overall flow balance. In variant A, the monitored outlets were defined as Q_{first}, Q_{leftI}, Q_{leftII}, Q_{rightI}, $Q_{rightII}$ and Q_{last}. In variant B, the outlets were arranged as Q_{leftI}, Q_{leftII}, $Q_{leftIII}$ and Q_{rightI}, $Q_{rightII}$ and $Q_{rightIII}$ reflecting the different inlet position and flow-division scheme. This monitoring approach enabled a direct comparison of the two configurations in terms of total flow rate and distribution of the working medium between the individual branches.

The mesh and simulation setup were defined to provide a consistent basis for comparing the two inlet-position variants. The discretisation was

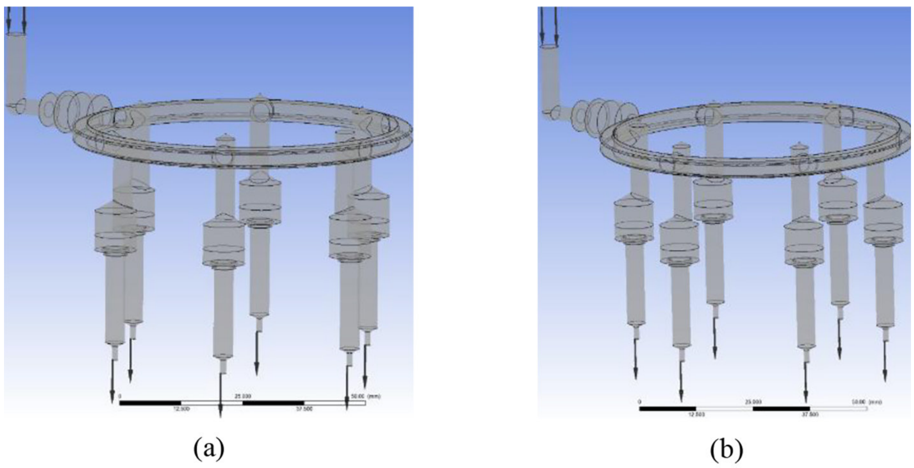

(a) (b)

Figure 8. Inlet and outlet boundary conditions in the CFX simulation: (a) inlet channel adjacent to one of the nozzle channels; (b) inlet channel located between the nozzle channels

Table 2. Simulation configuration summary

Parameter	(a) Inlet channel adjacent to the first nozzle channel/ (b) Inlet channel between nozzle channels I and II
Boundary conditions	
Analysis type	Steady-state
Material	Water, 18 °C, isothermal
Reference pressure	1 atm
Turbulence model	*k-ε* model, scalable wall functions
Advection scheme	High resolution
Convergence criterion	RMS = 1.0 × 10^{-4}
Surface: connection	Inlet total pressure (stable) = 6 bar
Surface: nozzle	Outlet average static pressure = 0 bar
Surface: wall	No-slip wall, smooth wall
Convergence settings (Solver Control)	
Timescale Factor	0.2
Minimum No. of iterations	111
Maximum No. of iterations	999
Monitor residuals	Full
Domain models	Non buoyant / Stationary

prepared with local refinement in regions relevant to internal-flow behaviour, including the inlet zone, nozzle supply channels, bends and near-wall regions. Identical boundary conditions, solver settings, flow-rate definitions and monitoring points were applied to both configurations. This approach enabled the influence of inlet location on pressure distribution, flow stability and nozzle supply uniformity to be assessed without introducing differences related to the numerical setup.

The numerical analysis included pressure and velocity fields, turbulence quantities, and time histories of the monitored nozzle and total flow rates. These results were used to evaluate flow stabilisation, identify possible disturbances within the manifold and compare the repeatability of medium distribution among the nozzle outlets.

The convergence behaviour of both inlet configurations was assessed using monitor plots for momentum and mass, turbulence quantities, individual nozzle flow rates and total flow rate. This enabled the stabilisation of the numerical solution to be verified before analysing the pressure and velocity fields.

In configuration A (Figure 9a), the initial flow response showed more pronounced disturbances and stronger oscillations, which can be attributed to the asymmetric supply of the working medium through the channel adjacent to one of the nozzles. After the initial transient phase, the monitored

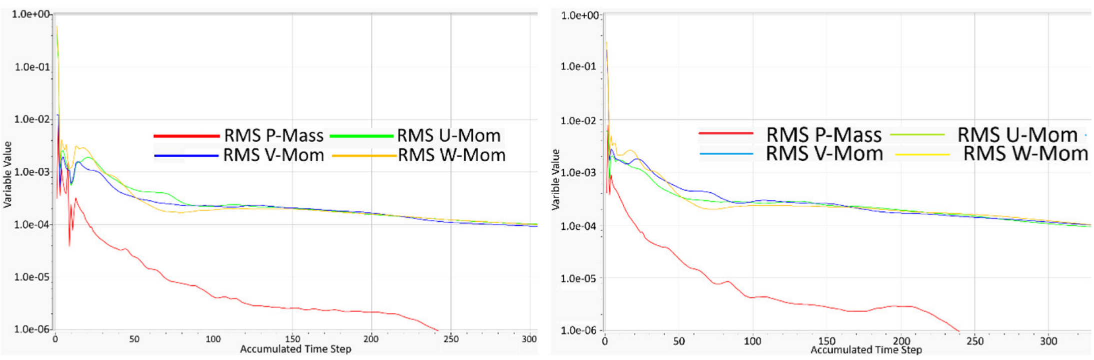

(a) (b)

Figure 9. Momentum and mass convergence plots: (a) inlet channel located adjacent to one of the nozzle supply channels; (b) inlet channel located between the nozzle supply channels

variables gradually approached a stable level, and the fluctuations progressively decreased. In configuration B (Figure 9b), the monitored profiles were more evenly distributed and the oscillations were damped more smoothly. This behaviour is associated with the inlet position between the nozzle channels, which promoted a more symmetrical flow division and reduced local disturbances. Since identical numerical settings were applied in both cases, the observed differences can be attributed mainly to the inlet geometry.

In configuration A (Figure 10a), the initial increase in turbulent kinetic energy was followed by a gradual decrease to a relatively stable level. In configuration B (Figure 10b), a rapid initial decrease was also observed; however, the intermediate part of the plot showed a more pronounced local increase and greater divergence between the monitored curves. This indicates a less uniform stabilisation process during the intermediate stage. Nevertheless, both configurations ultimately approached a similar level of convergence.

The nozzle flow-rate profiles for all monitoring points are shown in Figure 11. In both configurations, the monitored flow rates approached a quasi-steady level after a short transient phase, with no persistent oscillations in the final stage of the calculations. In configuration A, greater scatter between the curves was observed, indicating less uniform flow distribution among the nozzles. In configuration B, the profiles were more closely grouped, which indicates a more balanced distribution of the working medium. The enlarged plots support the assessment of the stabilisation process and make it possible to identify minor differences in the final flow-rate levels.

The monitor plots obtained during the simulation confirmed that both configurations were solved under comparable numerical conditions. Therefore, the subsequent analysis of pressure and velocity fields could be interpreted primarily in relation to the inlet geometry and its influence on the internal flow distribution.

RESULTS

To compare the distribution of the working medium within the developed head, the pressure and velocity fields were analysed using contour, streamline and vector plots. Particular attention was paid to the uniformity of nozzle supply, local pressure variations within the manifold, and the occurrence of regions of acceleration, stagnation or disturbed flow. The analysis was supplemented by a comparison of the outlet flow rates of the individual nozzles, which enabled a quantitative assessment of supply uniformity in both design variants.

In configuration A (Figure 12a), the pressure field shows a local region of elevated pressure near the inlet, followed by gradual pressure equalisation along the manifold. Although no abrupt pressure discontinuities are observed further downstream, a more pronounced asymmetry is visible in the inlet region and near the first branch, indicating a higher local hydraulic load. In configuration B (Figure 12b), the pressure field is distributed more uniformly around the manifold, with less pronounced dominance of one side of the system. This suggests a more balanced redistribution of flow energy and a lower tendency for local concentration of pressure losses near the inlet. In both configurations, the pressure field

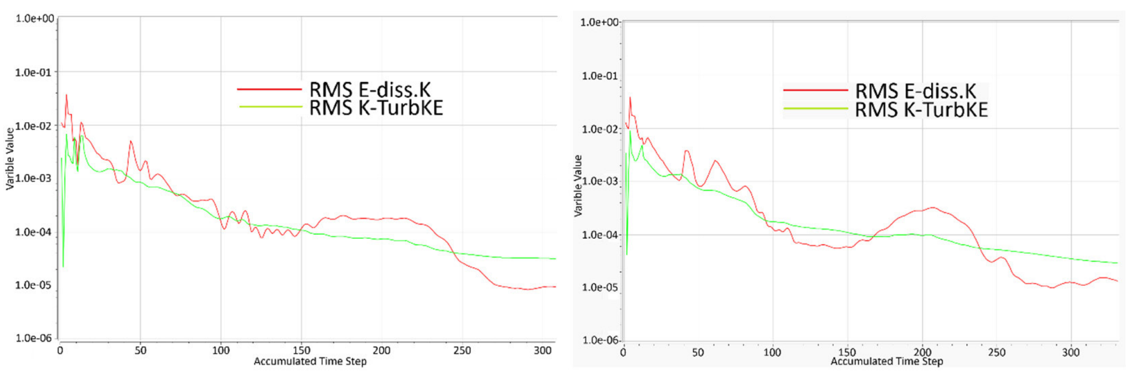

(a) (b)

Figure 10. Turbulent kinetic energy convergence plots: (a) inlet channel located adjacent to one of the nozzle supply channels; (b) inlet channel located between the nozzle supply channels

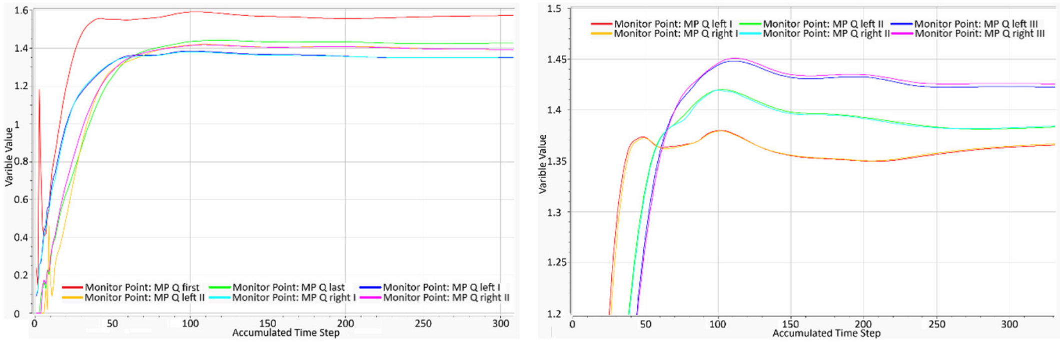

(a) (b)

Figure 11. Nozzle flow-rate monitor plots: (a) inlet channel located adjacent to one of the nozzle supply channels; (b) inlet channel located between the nozzle supply channels

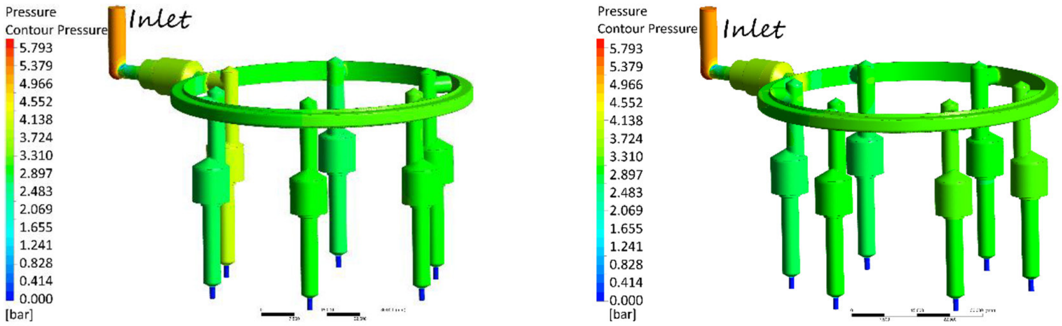

(a) (b)

Figure 12. Pressure contours: (a) inlet channel located adjacent to one of the nozzle supply channels; (b) inlet channel located between the nozzle supply channels

remains stable and no clear indication of adverse flow behaviour is observed. However, from the point of view of uniform nozzle supply, configuration B provides a more balanced pressure distribution within the manifold.

In configuration A, shown in isometric view in Figure 13a, the streamlines indicate an ordered flow pattern. Local acceleration and preferential supply to the nearest branches can be observed in the inlet region. Further along the manifold, the streamline pattern remains stable, with no clear evidence of flow separation or extensive recirculation zones. This indicates continuity of medium transport within the manifold.

In configuration B (Figure 13b), the streamlines are distributed more uniformly around the manifold. This indicates a more balanced supply to the branches and a lower tendency for local dominance of one side of the system. Both configurations show an ordered flow pattern without significant disturbances. However, configuration B provides a more symmetrical flow division within the manifold, understood as a more balanced hydraulic loading on both sides of the inlet and a more uniform distribution pattern along the ring.

In the isometric view (Figure 14), the velocity vector field shows an ordered flow pattern throughout the manifold. In configuration A, a higher concentration of vectors is visible near the inlet, which results from its position relative to the first branch. In configuration B, the vector distribution is more balanced over the manifold, indicating a greater degree of flow symmetry. In both cases, no clear recirculation structures or distinct stagnation zones are observed, which confirms that the internal geometry provides stable supply conditions for the nozzles.

In the side view (Figure 15), the flow within the main channel remains continuous and ordered, with no clear signs of abrupt directional changes that could increase local energy losses. In configuration A, stronger alignment of the velocity vectors is visible in the inlet region, indicating a higher hydraulic load in the initial section of the manifold. In configuration B, the velocity field is distributed more evenly around

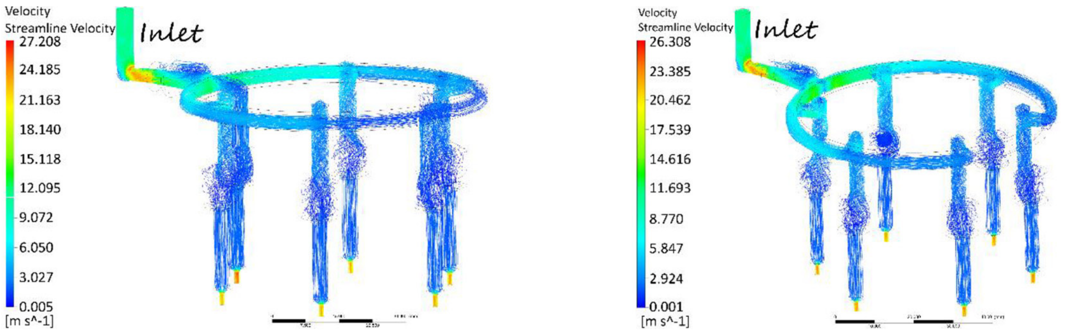

(a) (b)

Figure 13. Velocity streamlines in isometric view: (a) inlet channel located adjacent to one of the nozzle supply channels; (b) inlet channel located between the nozzle supply channels

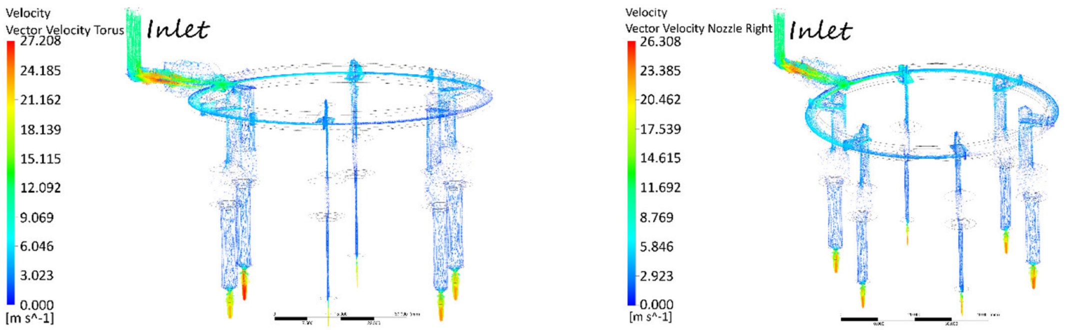

(a) (b)

Figure 14. Velocity vectors in isometric view: (a) inlet channel located adjacent to one of the nozzle supply channels; (b) inlet channel located between the nozzle supply channels

the manifold circumference. Both configurations provide stable flow conditions; however, configuration A is more consistent with the design assumption of preferential supply to the front zone of the robot.

In the top view (Figure 16), the distribution of flow energy among the individual branches is shown most clearly. In configuration A, the initial section of the manifold is more dominant, resulting in a greater proportion of the flow being directed towards the region closest to the inlet, whereas the more distant branches are supplied in a progressively more even manner. In configuration B, the vector distribution is more symmetrical with respect to the system axis. However, this does not correspond to a substantially different level of nozzle-supply uniformity, as the observed differences remain local rather than global.

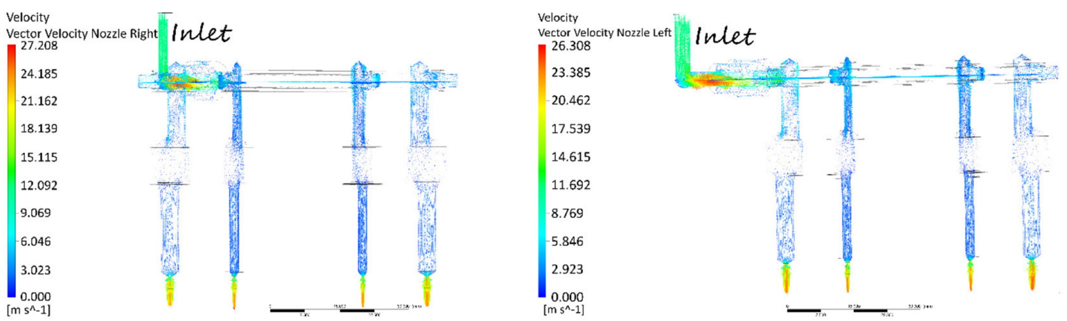

(a) (b)

Figure 15. Velocity vectors in side view: (a) inlet channel located adjacent to one of the nozzle supply channels; (b) inlet channel located between the nozzle supply channels

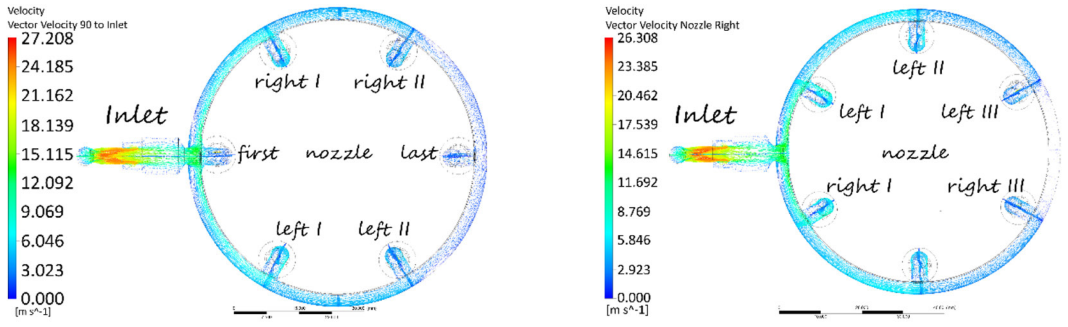

(a) (b)

Figure 16. Velocity vectors in top view: (a) inlet channel located adjacent to one of the nozzle supply channels; (b) inlet channel located between the nozzle supply channels

Overall, the analysis indicates that both configurations provide stable flow conditions without significant disturbances (Table 3). Configuration B provides a more balanced flow distribution within the manifold, whereas configuration A is more consistent with the design assumption of preferential supply to the front zone of the robot, corresponding to the direction of dispersion of material removed from the surface during operation

DISCUSSION

The numerical results showed that the inlet position in the compact manifold influenced the local pressure distribution, velocity field and flow-rate distribution across the nozzle outlets. Both analysed configurations provided stable internal flow conditions, without distinct stagnation zones, extensive recirculation regions or persistent flow disturbances. The total flow rates were comparable, indicating that the inlet location had a limited effect on the overall hydraulic capacity of the head. However, differences were observed in the local distribution of the working medium within the manifold.

Configuration B, with the inlet located between the nozzle channels, produced more balanced pressure and velocity distributions and reduced the dominance of one side of the manifold. This resulted in a more uniform supply of the individual nozzles. Configuration A generated greater local asymmetry near the inlet, but its flow pattern remained stable and may be advantageous when preferential supply to the front zone of the robot is required. Therefore, the selection of the manifold variant should consider both flow uniformity and the functional orientation of the head relative to the abrasive discharge zone.

The results indicate that the proposed compact manifold geometry is suitable for supplying six full-cone nozzles under the adopted boundary conditions. In comparison with more complex dust-suppression systems requiring additional dosing, charging or flow-control devices, the analysed solution is based on standard nozzles and a serviceable modular body. This

Table 3. Comparison of volumetric flow rates at individual nozzle outlets

Measurement point	(a) Inlet channel located adjacent to one of the nozzle supply channels [L/min]	(b) Inlet channel located between the nozzle supply channel [L/min]
First nozzle	1.571	-
Left nozzle I	1.350	1.365
Left nozzle II	1.392	1.383
Left nozzle III	-	1.422
Right nozzle I	1.351	1.366
Right nozzle II	1.392	1.384
Right nozzle III	-	1.426
Last nozzle	1.426	-
Total flow	8.481	8.347

supports its integration with a mobile magnetic robot, where mass, compactness and ease of maintenance are important design constraints. The CFD analysis enabled the differences between the inlet configurations to be identified before prototype testing, particularly in terms of pressure distribution, flow symmetry and nozzle-supply uniformity.

CONCLUSIONS

The study assessed two inlet-location variants of a modular water-curtain head intended for integration with a mobile magnetic robot used in abrasive blasting. The analysed head consisted of a compact manifold supplying six replaceable G1/8″ full-cone nozzles.

The CFD simulations performed using ANSYS CFX showed that both inlet configurations provided stable flow distribution within the manifold. No distinct stagnation zones, extensive recirculation regions or flow disturbances affecting nozzle-supply continuity were observed under the adopted boundary conditions.

The inlet position affected the local hydraulic behaviour of the head. Configuration B, with the inlet located between the nozzle channels, provided a more balanced pressure and velocity distribution and a more uniform nozzle supply. Configuration A, with the inlet located adjacent to one nozzle channel, produced greater local asymmetry near the inlet, but remained consistent with the assumption of preferential supply to the front zone of the robot.

The results indicate that CFD analysis is a useful tool for the design assessment of compact spraying heads before prototype testing. The developed water-curtain head provides a compact and serviceable solution to support dust suppression near the abrasive discharge zone without modifying the abrasive blasting process itself.

Acknowledgements

The mobile robotic system is covered by two patent applications concerning its key functional modules. Patent application P.436523 relates to the magnetic adhesion module based on a Halbach array adapted to curved ferromagnetic surfaces, whereas patent application P.451835 concerns the oscillatory–translational cleaning unit used for abrasive surface preparation.

REFERENCES

1. Qi C., Weinell C.E., Dam-Johansen K., Wu H. A review of blasting waste generation and management in the ship repair industry. Journal of Environmental Management. 2021;300:113714. https://doi.org/10.1016/j.jenvman.2021.113714
2. Jin F., Li S., Yang D., Wang S., Yang T., Liu Q., et al. Influence of atomization characteristics of hydrophilic SiO2 nanofluid on fine coal dust suppression performance. Fuel. 2026;417:138544. https://doi.org/10.1016/j.fuel.2026.138544
3. Xiong G., Ge S., Liu S., Zhao W., Sun L., Pang X. Magnetoelectric synergy enhances droplet wetting and capture of respirable hydrophobic coal dust: Mechanisms and suppression performance. Powder Technology. 2026;472:122152. https://doi.org/10.1016/j.powtec.2026.122152
4. Liu Z., Jiang B., Zhou Y., Pan G., Zhang Y., Wang Y., et al. Preparation and dust suppression performance of a chitosan-based composite dust suppressant for mining applications. Powder Technology. 2026;473:122211. https://doi.org/10.1016/j.powtec.2026.122211
5. Ding X., Xu Q., Liu F., Peng H., Wang Y., Ma M., et al. Unveiling the multi-droplet dynamics in dust suppression: a combined numerical and molecular dynamics study on the wetting, coating, and agglomeration using biomass-betaine surfactants. Journal of Environmental Management. 2026;403:129272. https://doi.org/10.1016/j.jenvman.2026.129272
6. Huang J., Zhang J., Wu Y., Zhao W., Gui X., Liu P. Engineering mitigation of submicron dust in high-altitude tunnels: investigation of the mechanism and development of an intelligent “Plateau Lung” suppression system. Tunnelling and Underground Space Technology. 2026;170:107400. https://doi.org/10.1016/j.tust.2025.107400
7. Wei Y., Wen Y., Liu K., Li K., Wang S., Liu Y., Jin L. Research and application of discrete foam-air curtain synergic system for dust suppression in tunnel construction.
8. Powder Technology. 2026;469:121762. https://doi.org/10.1016/j.powtec.2025.121762
9. Jiang Z., Jing D., Ma H., Ge S., Ren S. Synergistic dust suppression in fully mechanized mining faces: integrating negative pressure induction with supersonic atomization. Process Safety and Environmental Protection. 2026. https://doi.org/10.1016/j.psep.2026.108669
10. Selim M.Y.E., Ghannam M.T., Al Nuaimi S.K., Abdelsalam A., Mazrui H.A., Mohamed A.O., Ali M. Injection spray macroscopic visualization and structure of Jojoba biodiesel-water emulsion into an atmospheric chamber. Energy Reports. 2026;15:109054. https://doi.org/10.1016/j.egyr.2026.109054

11. Wang X., Wang P., Peng Y., Li Y., Luo Y., Li S. Mathematical model of dust suppression efficiency of ultrasonic dry fog nozzle in coal mine. Powder Technology. 2026;476:122382. https://doi.org/10.1016/j.powtec.2026.122382
12. Wu G., Wang P., Li Y., Chen Y., Li S. Structural optimization of a magnetized water spray dust reduction device. Journal of Cleaner Production. 2026;553:147993. https://doi.org/10.1016/j.jclepro.2026.147993
13. Mu X., Sun L., Liu S., Pang X., Ge S., Jing D., Zhang T. Study on plasma-activated supersonic water fog atomization and dust suppression performance. Process Safety and Environmental Protection. 2026;207:108404. https://doi.org/10.1016/j.psep.2026.108404
14. Wang C.-Y., Zhang H., Xue T., Fang L. A multi-factor CFD simulation to dust suppression in dynamic dynamic tunnel excavation. Tunnelling and Underground Space Technology. 2025;159:106458. https://doi.org/10.1016/j.tust.2025.106458
15. Zeng F., Jiang Z., Zhang G., Yang B., Wang M., Wang Y., et al. Application of similarity criteria in mechanistic study of spray-based dust suppression at open-pit truck unloading stations: Insights from scaled experiments and numerical simulations. Powder Technology. 2026;473:122239. https://doi.org/10.1016/j.powtec.2026.122239
16. Gao J., Wang J.-F., Zuo Z., Xu H., Xu H., Wang D., Zhang W. Application of wind-assisted electrospray for fugitive dust suppression in port coal unloading operation. Journal of Environmental Chemical Engineering. 2026;14:122032. https://doi.org/10.1016/j.jece.2026.122032
17. Chen Z., Zhao S., Dong C., Wang S., Guo Y., Gao X., et al. Spray dust control measures of tunnel blasting dust based on CFD dust-droplet coupling model and orthogonal test. Tunnelling and Underground Space Technology. 2025;156:106233. https://doi.org/10.1016/j.tust.2024.106233
18. Yang S., Ren J., Wan G., Ma F. Experimental study on wind-fog coupling dust suppression technology in tunnel drilling and blasting operations based on CFD numerical simulation. Chemical Engineering Research and Design. 2025;216:347-366. https://doi.org/10.1016/j.cherd.2025.03.001
19. Yang T., Shao H., Cheng J., Li W., Si J., Qi S. Influence of nozzle structure on atomization characteristics and coal dust suppression efficiency of siphon aerodynamic atomizing nozzle. Powder Technology. 2026;474:122250. https://doi.org/10.1016/j.powtec.2026.122250
20. Chen X., Zhang J., Tong L., Li X., Fang L., Liang Y., et al. Mechanism of wind-responsive dust suppression parameter adjustment and feedforward control system for fog gun in open-pit mine loading areas. Powder Technology. 2026;476:122413. https://doi.org/10.1016/j.powtec.2026.122413
21. Zhang S., Nie W., Guo C., Peng H., Ma Q., Xu C., et al. Optimization of spray dust suppression device in return air tunnel of a coal mine based on CFD technology. Building and Environment. 2021;203:108059. https://doi.org/10.1016/j.buildenv.2021.108059
22. Kang M., Jang I., Song S. Effects of header design on thermal characteristics of multi-nozzle steam spraying. International Journal of Heat and Fluid Flow. 2024;106:109291. https://doi.org/10.1016/j.ijheatfluidflow.2024.109291
23. Pac P., Tokarczyk J., Prostański D., Sękala A., Rosikowski P. Alternatywna metoda analizy wyników symulacji MES w oprogramowaniu CAD bez zaawansowanych narzędzi postprocesingu. In: Interdyscyplinarne badania młodych naukowców. Gliwice: Wydawnictwo Politechniki Śląskiej; 2023. p. 330–344 [in polish].
24. Pac P., Prostański D. Optimization of the topology of the structural component of a magnetic robot. Mining Machines. 2024;42:30–48.
25. Pac P., Prostański D., Sękala A. Verification and calibration of FEM for a magnet-robot frame using virtual strain gauges-experimental and analytical procedure. In: Interdisciplinary Research of Young Scientists. Gliwice: Wydawnictwo Politechniki Śląskiej; 2025. p. 60–76.
26. Pac P., Prostański D., Sękala A. Virtual strain gauges-fast experimental validation of FEM for a magnet-robot frame. In: Proceedings of InterTechDoc'25; 2025 Sep 15–17; Zabrze, Poland.
27. Spraying Systems Co. B1/8HH-SS2 FullJet® full cone nozzle. Available from: https://portal.spray.com/en-eu/products/b1-8hh-ss2. Accessed 22 Mar 2026.
28. OpenStax. University Physics Volume 1. Houston: OpenStax; 2016.